ELSEVIER

Sensors and Actuators A 88 (2001) 178–186

SENSORS AND ACTUATORS A PHYSICAL
www.elsevier.nl/locate/sna

System modeling of microaccelerometer using piezoelectric thin films

Jyh-Cheng Yu*, Chin-Bing Lan

Department of Mechanical Engineering, National Taiwan University of Science and Technology, 43 Keelung Road, Section 4, Taipei 106, Taiwan, ROC

Received 5 October 1999; received in revised form 28 August 2000; accepted 9 September 2000

Abstract

This paper addresses the system modeling of a novel design of microaccelerometer. The proposed microaccelerometer consists of a quadri-beam suspension, a seismic mass, and the displacement transducers using piezoelectric thin films. The derivation of the electromechanical system function illustrates the interactions of the material characteristics, the amplification circuit design, and the microstructure geometry. The dynamic response and the trade-off between several design considerations are discussed. The theoretical model is verified by the finite element analysis of the resonance frequency, the dynamic response of the microstructure, and the sensor sensitivity. The good coincidence of the results demonstrates the validity of the modeling assumptions. The analytical model can be readily applied to performance trade-off and design optimization. © 2001 Elsevier Science B.V. All rights reserved.

Keywords: MEMS; Microsensor; Piezoelectric accelerometer; Piezoceramic

1. Introduction

Relevant researches of micro-electromechanical systems (MEMS) have emerged in recent years as a result of the urge of product miniaturization. Microsensors are essential to the integration of electric and mechanical systems, and are the first commercialized MEMS products. The advance of micromachining has made possible the production of three-dimensional dynamic microstructures on a silicon wafer. Microsensors consist of microstructures, displacement transducers, and signal amplifiers, which can then be easily integrated into a single chip using existing integrated circuit manufacturing processes. The miniaturization of sensors not only reduces the manufacturing cost but also improves the operational bandwidth and reliability. The integration of electric and mechanical components facilitates the applications with space constraints. Successful applications in automotive engineering include pressure microsensors in combustion control, microaccelerometers in airbags and suspension systems [1], and micro-gyroscopes in navigation and guidance. Potential markets also exist in biomechanics and aerospace technology.

Accelerometers can be classified into the following categories according to the forms of transduction mechanism [2]: piezoresistive [3]; capacitive [4]; resonant [5]; tunneling [6]; thermal [7]; optical [8]; piezo-MOS [9]; and piezoelectric [10] devices. Piezoresistive and capacitive based transducers are most popular in micromachined silicon accelerometers. One of the first commercialized microaccelerometers was piezoresistive. The main advantage of piezoresistive accelerometers is the simplicity of their structure, fabrication process, and read-out circuitry. However, piezoresistive accelerometers show high temperature dependence and a great influence of mounting stress. Capacitive accelerometers have good dc response and noise performance, low temperature sensitivity, and low drift, but have problems with electromagnetic interference. In another way, novel deigns, such as those based on tunneling current or optical read-out, can achieve high sensitivity with a small size; however, none of these has been commercialized to date. Piezoelectric accelerometers have the advantages of easy integration in existing measuring systems. Due to their excellent dynamic performance and linearity, they have been widely used in condition monitoring systems to measure machinery vibration [11].

Piezoelectric materials have the interchangeability of electrical and mechanical energy. The most widely used piezoelectric ceramics are $PbZrTiO_6$ solid solutions (PZT). Because of the advantages of their high electro-mechanical coupling factors, high electric impedance, and temperature stability, piezoelectric transducers are very promising in sensor and actuator applications [12]. Piezoelectric thin films keep the characteristics of bulk materials, but are more compact and less costly. The quality of thin films used to be a

* Corresponding author. Tel.: +886-2-27376499; fax: +886-2-27376499.
E-mail address: jcyu@mail.ntust.edu.tw (J.-C. Yu).

0924-4247/01/$ – see front matter © 2001 Elsevier Science B.V. All rights reserved.
PII: S0924-4247(00)00502-1

constraint in the application of micro-transducers. However, continuous breakthroughs in coating processes for ceramic thin films have greatly improved the films' quality, which has drawn lots of research interests [13].

Many literatures focus on the manufacturing aspects of microsensors [14,15]. Some conduct FEM analysis of the thin film on a flexible structure subject to bending moment, torsion, and transverse shear to study the influence of structure stresses on the static and dynamic piezoelectric properties [16]. Vaz [17] derives the interaction equations for a flexible beam with multiple-bonded piezoelectric films, which is useful for shape control and active vibration damping in flexible structure. van Kampen and Wolffenbuttel [18] conduct an extensive modeling of seismic microstructure to illustrate the mechanical behavior of bulk-micromachined silicon accelerometers. Nemirovsky et al. [19] design and analyze a compression type piezoelectric thin-film accelerometer. No single configuration can meet all the measurement requirements. Design for performance trade-off is necessary for various applications. However, studies on the modeling and parameter design of sensor systems are few. This paper aims to model the dynamics of the flexible structures with piezoelectric films and to illustrate the interactions among the microaccelerometer design variables.

2. Typical model of piezoelectric accelerometer

Fig. 1 represents a general configuration of a seismic-displacement pick up for unidirectional translation. The system consists of a mass-spring-damper structure and a displacement transducer. The acceleration $\ddot{x}_i$ of the moving object is the physical quantity under investigation, which introduces a deflection of the microstructure. The displacement transducer picks up the deflection and converts it to an electric signal. The complete system can be divided into a mechanical subsystem G_m and an electric subsystem G_e.

2.1. Mechanical subsystem

The mechanical transfer function G_m models the frequency response of the relative displacement x_o of the seismic mass and the sensor base due to the acting acceleration $\ddot{x}_i$. According to Newton's second law, the governing equation of the seismic mass M at small displacement is as follows:

$$M\ddot{x}_i = M\ddot{x}_o + B\dot{x}_o + Kx_o \quad (1)$$

Assuming the initial conditions: $x_o(0) = 0$ and $\dot{x}_o(0) = 0$, manipulation of the Laplace transformation of Eq. (1) gives the mechanical transfer function

$$G_m(s) = \frac{x_o(s)}{\ddot{x}_i(s)} = S_m \frac{\omega_n^2}{s^2 + 2\zeta\omega_n s + \omega_n^2} \quad (2)$$

where $\omega_n = \sqrt{K/M}$ is the resonance frequency of the structure, $\zeta = B/2\sqrt{KM}$ the damping ratio, and $S_m \equiv M/K$ the mechanical sensitivity.

The square of the resonance frequency, ω_n^2, is in proportion to the spring stiffness, K, and in inverse proportion to the seismic mass, M. On the contrary, the mechanical sensitivity, S_m, is in proportion to M and in inverse proportion to K. Sensor designs need to trade-off between the increase of the resonance frequency to widen the operational frequency bandwidth and the increase of the mechanical sensitivity to enhance the sensing resolution.

2.2. Electric subsystem

The electronic transfer function G_e models the frequency response of the relative displacement x_o and the output voltage e_o of the displacement transducer. In general, the electric transfer system includes a piezoelectric transducer, connecting cables, and a charge amplifier. The piezoelectric transducer assumes a linear transformation between the output charge and the relative displacement x_o of the seismic mass and the sensor base.

$$Q = K_q x_o \quad (3)$$

where K_q is the charge output of unit displacement.

Fig. 2 represents the analogous circuit of the transducer subsystem that can be simplified to the equivalent model in Fig. 3 [20]. Both the transducer and the amplifier have high impedance to prevent the leakage of the electric charge. The resulting resistance and capacitance of the equivalent model are shown in Eqs. (4) and (5) where R_{leak} is often much larger

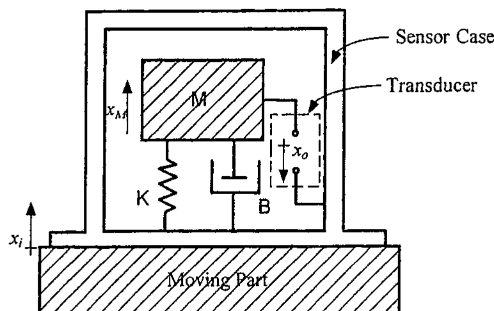

Fig. 1. Typical system model of an accelerometer.

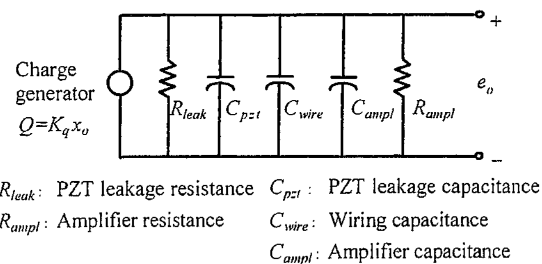

Fig. 2. Typical model of piezoelectric transducer subsystem.

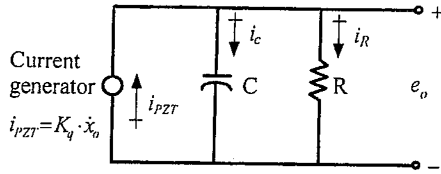

Fig. 3. Equivalent circuit of piezoelectric transducer subsystem.

than R_{ampl}.

$$R \equiv \frac{R_{\mathrm{ampl}} R_{\mathrm{leak}}}{R_{\mathrm{ampl}} + R_{\mathrm{leak}}} \approx R_{\mathrm{ampl}} \tag{4}$$

$$C \equiv C_{\mathrm{PZT}} + C_{\mathrm{wire}} + C_{\mathrm{ampl}} \tag{5}$$

Analysis of the equivalent circuit will yield the governing equation of the electric subsystem.

$$C\left(\frac{\mathrm{d}e_{\mathrm{o}}}{\mathrm{d}t}\right) = i_{\mathrm{PZT}} - i_{\mathrm{R}} = K_{\mathrm{q}}\left(\frac{\mathrm{d}x_{\mathrm{o}}}{\mathrm{d}t}\right) - \frac{e_{\mathrm{o}}}{R} \tag{6}$$

$$\dot{e}_{\mathrm{o}} = \frac{K_{\mathrm{q}}}{C}\dot{x}_{\mathrm{o}} - \frac{e_{\mathrm{o}}}{\tau} \tag{7}$$

where $\tau \equiv RC$ is the time constant. The electric transfer function of the transducer subsystem is as follows:

$$G_{\mathrm{e}}(s) = \frac{e_{\mathrm{o}}(s)}{x_{\mathrm{o}}(s)} = S_{\mathrm{e}}\frac{\tau s}{\tau s + 1} \tag{8}$$

where $S_{\mathrm{e}} \equiv K_{\mathrm{q}}/C$ is the electric sensitivity.

2.3. System model of piezoelectric accelerometer

The complete system model combines the mechanical and electric transfer functions as follows:

$$\frac{e_{\mathrm{o}}(s)}{\ddot{x}_{\mathrm{i}}(s)} = S_{\mathrm{T}}\frac{\tau s}{\tau s + 1}\frac{\omega_{\mathrm{n}}^2}{s^2 + 2\zeta\omega_{\mathrm{n}}s + \omega_{\mathrm{n}}^2} \tag{9}$$

where $S_{\mathrm{T}} \equiv S_{\mathrm{e}}S_{\mathrm{m}} = (K_{\mathrm{q}}/C)(M/K)$ is the sensitivity of sensor.

The typical range of the accelerometer frequency response, using ±5% as an accuracy requirement, is between $3/\tau$ and $\omega_{\mathrm{n}}/5$ (Fig. 4). The low-frequency response is limited by the time constant τ of the piezoelectric transducer while the high-frequency range is limited by mechanical resonance ω_{n}. It is impossible for a piezoelectric accelerometer to measure a static acceleration since the charge will leak away across the resistance of the sensor and the input resistance of the amplifier. Through a care circuitry design, the piezoelectric accelerometer can present a near dc response [19]. On the other hand, the piezoelectric characteristic, K_{q}/C, and the structure characteristic, $1/\omega_{\mathrm{n}}^2$, determine accelerometer sensitivity. Therefore, trade-offs exist between high frequency response and sensitivity.

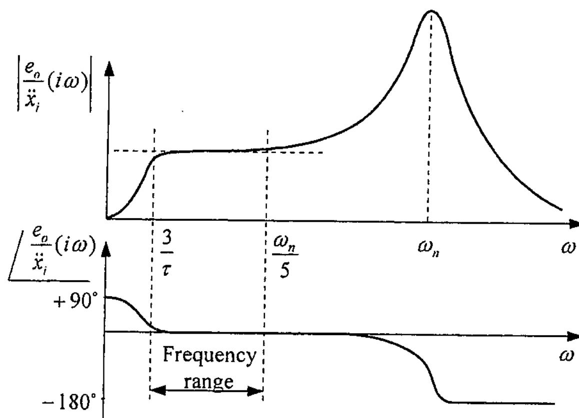

Fig. 4. Piezoelectric accelerometer frequency response.

3. Derivation of parametric system model

3.1. Static behavior of microstructure

There are three basic modes of piezoelectric transducers: compression mode, shear mode, and bending mode (or cantilever mode). Fig. 5 shows the corresponding structures of piezoelectric accelerometer. Bending mode transducers have a better sensitivity and manufacturability for micro-accelerometers using piezoelectric thin films. The following section will focus on the modeling of the bending type piezoelectric microaccelerometer.

Fig. 6 shows four basic suspension configurations of bending mode piezoelectric microaccelerometers. When some acceleration is acting on the structure, the seismic masses using suspension of one and two beams are subject to rotations along x-axis and y-axis in addition to the translation along z-axis. On the other hand, the centered seismic mass suspended by four symmetric beams, as shown in Fig. 6(d), will only vibrate along z-axis with negligible motions in other directions. This configuration will greatly simplify the modeling process. Although tension stresses present in addition to bending stresses of suspension beam, which might affect the linearity of accelerometer, the effect is negligible for small displacements.

This paper adopts the microaccelerometer configuration of four symmetric beam suspensions with eight piezoelectric transducers arranged as shown in Fig. 7. The piezoelectric transducer is composed of an upper electrode, a piezoelectric thin film, and a lower electrode. Each suspension beam are attached two transducers. One is near the fixed end and the other is near the seismic mass. In the first vibrating mode of the beam, the stresses of the inner and the outer transducers due to bending of the beam are in the opposite direction. On the other hand, the stresses due to unexpected

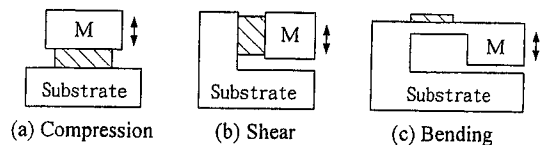

Fig. 5. Basic structures of piezoelectric accelerometers.

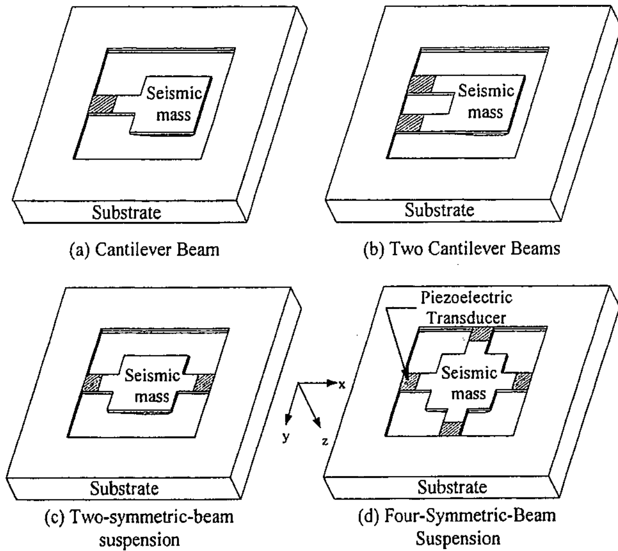

Fig. 6. Basic suspension configurations of piezoelectric microaccelerometers.

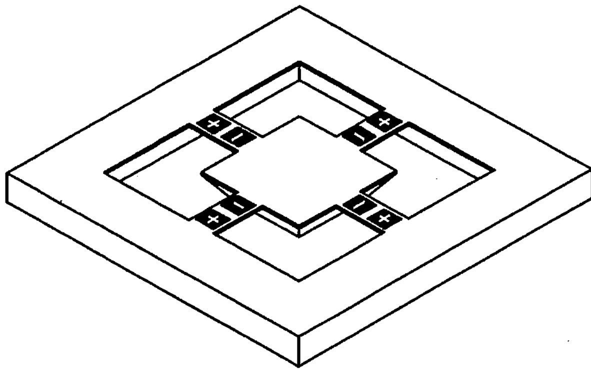

Fig. 7. A 3-D view of the proposed microaccelerometer.

noises, such as accelerations in x and y directions, and the tensions of the deflective beams, are in the same direction. The upper electrodes of the outer transducers are connected with the lower electrodes of the inner transducers, and the lower electrodes of the outer transducers are connected with the upper electrodes of the inner transducers, as shown in Fig. 7. These noise effects will then be cancelled out. This design not only increases the transducer sensitivity, but also reduces the noise effects.

The conventional material coordinate system uses a different notation from the mechanics coordinate system. Consider the rectangular piezoelectric film illustrated in Fig. 8. The 1-axis and 2-axis define a plane that is parallel to the film's surface. The 3-axis is perpendicular to the film's surface and points in the opposite direction to the electric field used to pole the piezoelectric film during its manufacture. The material coordinates 1–2–3 are arranged to coincide with the mechanical coordinates x–y–z in the following analysis.

The mechanical model of the accelerometer is based on the following assumptions:

1. The weight of the supporting beams is negligible compared with the seismic mass.
2. The seismic mass and rim of the structure are rigid.
3. The deflections of supporting beams observe linear elasticity and Hooke's law.
4. The seismic mass only vibrates in the z-axis.
5. The piezoelectric films and electrodes are much thinner than supporting beams, and have negligible effect on the beams' stiffness.

The dimensions of the transducer are illustrated in Fig. 8. The placements of the transducers are slightly away from the fixed and the seismic ends to avoid the stress nonlinearity due to finite rigidity. Also, the middle section of the beam is not suitable for transducer placement because of low sensitivity. Chen et al. [10] has shown that the signal-to-noise ratio (SNR) will be improved by reducing the electrode area, thus only covering the beam area of high bending stresses. The optimum placement design is left for future study.

When the sensor is subject to a normal acceleration, $\ddot{z}_i$, the inertial force of the seismic mass induces a deflection of the beam suspension. The relative displacement of the seismic mass and sensor base is z_s. Consider only the first mode vibration. The free-body diagram of one of the supporting beams will look like Fig. 9. The mid-point, C, of the supporting beam will deflect half the distance measured at the seismic mass because of symmetry.

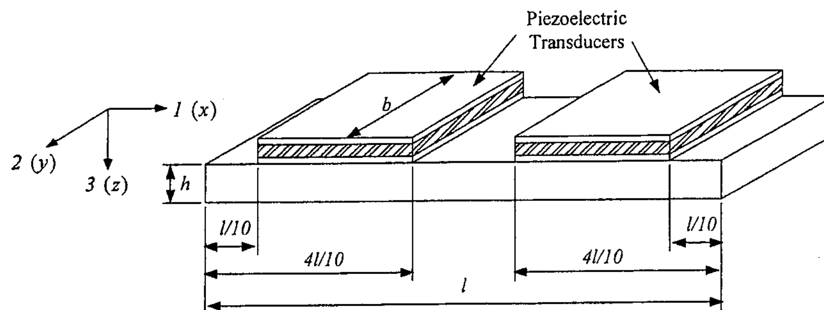

Fig. 8. Details of beam suspension and piezoelectric transducers.

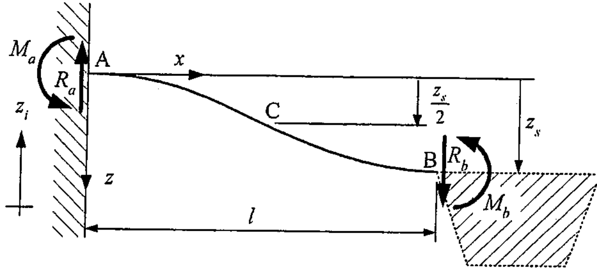

Fig. 9. Free-body diagram of suspension beam.

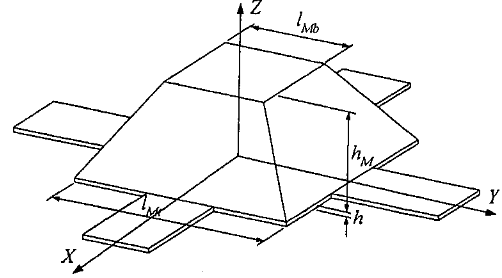

Fig. 10. Details of the pyramid shaped seismic mass.

The bending moment M_x in the beam at location x is given by

$$M_x = R_a x - M_a \tag{10}$$

If the deflection is small, the differential equation of the deflection of beam is approximated according to Hooke's law as follows:

$$\frac{d^2 y}{dx^2} = -\frac{M}{EI} \tag{11}$$

where $I = 1/12\, bh^3$ is the moment of inertia of the rectangular beam, and E the elastic modulus of silicon.

Solving the differential equation with the boundary conditions yields

$$M(x) = \frac{12EIz_s}{l^3}x - \frac{6EIz_s}{l^2} \tag{12}$$

Assume the bonding between the piezoelectric film and beam suspension is perfect. When the inertial force of the seismic mass is acting on the beam, the strain on the piezoelectric film is approximately equal to the upper surface strain of the bonded beam. The stresses of the piezoelectric film in the 1 direction can be obtained as follows:

$$T_1 = c_{11}S_1 - \nu c_{12}S_1 \approx \frac{hz_s(c_{11} - \nu c_{12})}{l^2}\left(3 - \frac{6x}{l}\right) \tag{13}$$

where c is the stiffness coefficient, $S_1 = M(x)(h/2)/I$ the strain, and ν the Poisson's ratio of the piezoelectric film. Since the seismic mass is supported by four beams, the total reaction force is $F = 4R_a$. The stiffness K of the beam suspension is

$$K = \frac{48EI}{l^3} \tag{14}$$

3.2. Seismic mass

When using bulk-micromachining techniques, the seismic mass is shaped like a truncated pyramid, as shown in Fig. 10, due to the anisotropic etching of silicon in KOH [21]. Prior research has revealed that etching of convex corners is mainly due to etching of {4 1 1} planes. Corner compensation structures in the design of masking layer have to be used to realize the shape of the mass [22]. Neglect the imperfection of convex corner compensation and simple integration of the structure will give the mass

$$M = \frac{\sqrt{2}\rho}{6}[l_{Mt}^3 - (l_{Mt} - \sqrt{2}h_M)^3] + \rho l_{Mt}^2 h \tag{15}$$

where ρ is the density of silicon.

3.3. System transfer function

The mechanical subsystem of the piezoelectric microaccelerometer is similar to Eq. (2) with the sensitivity S_m is as follows:

$$S_m \equiv \frac{M}{K} = \frac{Ml^3}{48EI} = \frac{Ml^3}{4Ebh^3} \tag{16}$$

If the piezoelectric films are subject to stresses in the 1 direction, and the stresses in other directions (T_2, T_3, T_4, T_5, and T_6) are all negligible. The contribution from an infinitesimal portion of the piezoelectric material to the total charge for no external electrical field is as follows:

$$D_3 = d_{31}T_1 \tag{17}$$

Substituting Eq. (13) into the integration of Eq. (17) along one suspension beam yields the charge output of piezoelectric films

$$Q = \int_{(1/10)l}^{(4/10)l} (D_3 b)\,dx - \int_{(6/10)l}^{(9/10)l} (D_3 b)\,dx = \frac{9d_{31}bhz_s(c_{11} - \nu c_{12})}{10l} \tag{18}$$

If the electrodes of four supporting beams are connected according to the transducer layout in Fig. 7, analogous to Eq. (3), the output charge of the piezoelectric transducer due to unit displacement of seismic mass is

$$K_q = \frac{18d_{31}bh(c_{11} - \nu c_{12})}{5l} \tag{19}$$

Substituting Eqs. (16) and (19) into Eq. (9) yields the system transfer function of the piezoelectric accelerometer.

$$\frac{e_o(s)}{\ddot{z}_i(s)} = S_T \frac{\tau s}{\tau s + 1} \frac{\omega_n^2}{s^2 + 2\zeta\omega_n s + \omega_n^2} \tag{20}$$

where $S_T = 9Md_{31}l^2(c_{11} - \nu c_{12})/10Eh^2C$ is the sensor sensitivity.

The accelerometer sensitivity S_T is mainly related to the dimensions of beam suspension, the transverse piezoelectric charge to stress ratio d_{31}, seismic mass, and the equivalent capacitance of the electric subsystem. The parameter designs of piezoelectric microaccelerometers depend on the features of performance desired for particular applications.

3.4. Noise analysis

The damping resistance, B, causes the mechanical–thermal noise in the mechanical subsystem of the accelerometer. In general, the minimum detectable acceleration is determined by the mechanical–thermal noise. The noise equivalent acceleration spectral density of the mechanical–thermal noise is given by [23]

$$S_n^{mt} = \frac{4k_B TB}{M^2}\left[\frac{(m/s^2)^2}{Hz}\right] \quad (21)$$

Gabrielson [23] derived the signal-to-noise ratio (SNR) of the subsystem

$$SNR = \frac{a_s{}^2 MQ}{4k_b T\omega_n} \quad (22)$$

where a_s is the magnitude of the input acceleration, k_B the Boltzmann constant (1.38×10^{-23} J/K), T the absolute temperature, and Q the quality factor of the mechanical subsystem.

$$Q = \frac{1}{2\zeta} = \frac{\sqrt{KM}}{B} \quad (23)$$

The acceleration magnitude a_s of the sinusoidal input, with magnitude X_s and frequency, ω, is $\omega^2|X_s|$.

The SNR can be improved by increasing the Q, reducing the resonance frequency ω_n, or increasing the mass M (which also lowers ω_n). The relation shows the advantage of bulk micromachining over surface micromachining since large seismic masses are more easily produced with bulk micromachining. The piezoelectric transducer has another advantage in the damping because it does not need to be in close proximity to another substrate, which leaves only the viscous damping due to air drag and damping due to the materials internal loss. Monocrystalline silicon has potentially low damping because of low internal friction. Smaller damping means a higher Q, which also improves the SNR.

The read-out electronics noise is the major concern in the electric subsystem. If a simple trans-impedance stage is used, the noise can be easily modeled from the equivalent resistor. The $1/f$ of the CMOS op-amp can be neglected due to the "high-pass" like behavior of the piezoelectric transducer. By using a low-noise op-amp, the electrical noise equivalent acceleration spectral density can be approximately given by

$$S_n^e = \frac{4k_B T}{R(S_T)^2}\left[\frac{(m/s^2)^2}{Hz}\right] \quad (24)$$

If a charge amplifier is used, more complicated noise scheme and the addition of a KTC noise will be involved. Depending on the design of the amplification circuit, the thermal–mechanical noise may be negligible compared to the electrical equivalent noise.

4. FEM analysis of frequency response

The proposed model of the mechanical behavior of microaccelerometers assumes the mass of the beam suspension and the stiffness of the electrodes and the piezoelectric films are negligible. This session introduces a finite element analysis using ANSYS 5.3 to verify the frequency response of the microstructure and the piezoelectric sensor. Table 1 shows the microstructure dimensions of the numerical example. Tables 2 and 3 list the typical material properties of the microstructure. The material properties of the thin film PZT layer have not yet been determined and hence the values of the bulk PZT 52/48 are used in the FEM analysis. The stiffness coefficient matrix is shown in Eq. (25).

$$[C]^E = \begin{bmatrix} 11.425 & 5.8294 & 5.8525 & 0 & 0 & 0 \\ 5.8294 & 11.425 & 5.8525 & 0 & 0 & 0 \\ 5.8525 & 5.8525 & 9.8181 & 0 & 0 & 0 \\ 0 & 0 & 0 & 2.0747 & 0 & 0 \\ 0 & 0 & 0 & 0 & 2.0747 & 0 \\ 0 & 0 & 0 & 0 & 0 & 2.6042 \end{bmatrix} \times 10^{10} \quad (25)$$

Fig. 11 shows the FEM model of the microstructure bonded with electrodes and PZT films. The ends of the supporting beams are assumed rigid. Because of the symmetry of configuration, a quarter of the microstructure is used to reduce the computational expense.

Table 1
Microstructure dimensions of the piezoelectric accelerometer

Length of beam suspension (l) (μm)	400
Width of beam suspension (b) (μm)	200
Thickness of beam suspension (h) (μm)	15
Length of seismic mass (l_{Ml}) (μm)	800
Thickness of seismic mass (h_M) (μm)	300
Thickness of PZT film (h_p) (μm)	0.3
Thickness of electrode (h_e) (μm)	0.2

Table 2
Mechanical properties of the piezoelectric accelerometer materials

	Material	Young's modulus (N/m^2)	Density (kg/m^3)	Poisson's ratio
Mechanical microstructure	Silicon	1.69×10^{11}	2330	0.0625
Piezoelectric film	PZT	Eq. (25)	7550	0.3
Electrodes	Platinum	171×10^9	2145	0.39

Table 3
Typical values of some material properties of bulk PZT

Dielectric constant ($\times 10^{-9}$ F/m)	
ε_{11}	10.443
ε_{22}	10.443
ε_{33}	6.4605
Piezoelectric coefficient ($\times 10^{-12}$ C/N)	
d_{31}	−93.5
d_{33}	223
d_{15}	494

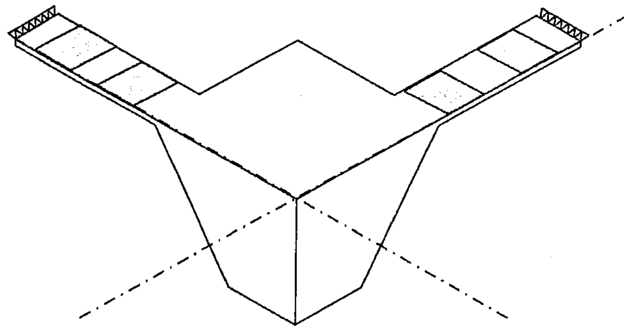

Fig. 11. FEM meshed model of the structure of microaccelerometer.

4.1. Resonance frequency

The resonance frequency is the structure characteristic that is independent to acting loads. The undamped resonance frequency of the microstructure in Hertz can be estimated from the proposed model as follows:

$$f_n = \frac{1}{2\pi}\sqrt{\frac{K}{M}} \tag{26}$$

where K and M are from Eqs. (14) and (15).

The modeling result gives the undamped resonance frequency 26,313 Hz which is very close to the peak frequency 26,218 Hz obtained from the FEM analysis.

4.2. Mechanical frequency response

The mechanical subsystem from the previous analysis is as follows:

$$\frac{z_s(s)}{\ddot{z}_i(s)} = \frac{Ml^3}{4Ebh^3}\frac{w_n^2}{s^2 + 2\zeta w_n s + w_n^2} \tag{27}$$

Table 5
Comparison of the sensor sensitivity before amplification

	Modeling result	FEM analysis
Sensor sensitivity (mV/g)	0.025	0.024

The FEM analysis assumes a harmonic acceleration motion along the z direction of the microstructure. The upper bound of the frequency range of the proposed microaccelerometer is approximately $\omega_n/5$. The input signal of the FEM analysis is then selected to be a unit harmonic acceleration, 1 m/s^2, with the frequency changed from 100 to 5000 Hz to verify the modeling result. Table 4 compares the frequency responses of the seismic mass displacement of the modeling result and FEM analysis.

4.3. Sensor sensitivity

The calculated and the FEM estimated sensitivities of the proposed accelerometer before signal amplification are given in Table 5.

The comparisons of the resonance frequency, the frequency response of seismic displacement, and the sensor sensitivity justify the previous modeling assumptions. Though the FEM analysis might provide a better estimate of the actual responses, the computation is expensive. The proposed model provides good estimations of sensor responses and illustrates the interaction of design variables and parameters. It can be readily applied to the parameter design of the piezoelectric microaccelerometer where design iterations are required.

4.4. Noise performance

The theoretical minimum detectable signal, $a_{\min}$, due to Brownian noise can be found be setting the SNR of Eq. (22) to unity and solving for $a_{\min}$.

$$a_{\min} = \sqrt{\frac{4k_b T\omega_n}{MQ}} \tag{28}$$

The seismic mass is about 0.274 mg. Assume the quality factor $Q = 0.707$, the detection level at room temperature is 1.2×10^{-4} m/s^2/Hz$^{1/2}$. The noise needs to be added by the read-out electronics noise. The mechanical–thermal noise level of the accelerometer design using bulk machining is

Table 4
Comparison of the frequency response of the seismic amplitude

Loading frequency (Hz)	Modeling response ($\times 10^{-11}$ m/m/s^2)	FEM analysis ($\times 10^{-11}$ m/m/s^2)	Difference (%)
100	3.8491	3.8429	0.16
300	3.8495	3.8434	0.16
500	3.8505	3.8443	0.16
1000	3.8549	3.8487	0.16
3000	3.9023	3.8957	0.17
5000	4.0008	3.9933	0.19

usually much lower than the required detection level. In this case, the read-out electronics noise will determine the accelerometer resolution. The electrical equivalent noise depends on the amplification circuit design. The charge sensitivity of the accelerometer due to the input acceleration is given by $S_m K_q$. Once the charge noise of the read-out electronics is determined, the detection level can be obtained by dividing the charge noise by the charge sensitivity.

5. Conclusion

This paper models the electromechanical system dynamics of the microaccelerometer using piezoelectric films. A configuration of multiple-supported microstructure is proposed to derive the design variables and parameters. The mechanical and electric subsystems are elaborated to illustrate the interactions of material characteristics, amplification circuit design, and structure geometry. Discussions of sensor performance trade-off are presented. The numerical example shows the advantage of the design. The FEM analysis of the frequency response of the accelerometer coincides with the modeling results, which demonstrates the potential applications of the system model to the microaccelerometer parameter design. Since the parametric models of the sensor sensitivity, the frequency bandwidth, and the detection level are derived, optimal designs of the geometrical dimensions can be readily achieved. Also, manufacturing errors, such as micromachining tolerances and material uncertainty, would lead to a quality problem, which needs to be addressed before the realization of the sensor mass production. Future study could include design optimization and performance robustness of the accelerometer [24].

Acknowledgements

This research is funded by the National Science Council of the ROC under grant NSC 88-2216-E-011-013.

References

[1] G.A. Macdonald, A review of low cost accelerometers for vehicle dynamics, Sens. Actuators A21–A23 (1990) 303–307.
[2] N. Yazdi, F. Ayazi, K. Najafi, Micromachined inertial sensors, Proc. IEEE 86 (8) (1998) 1640–1659.
[3] H. Chen, S. Shen, M. Bao, Over-range capacity of a piezoresistive microaccelerometer, Sens. Actuators 58 (3) (1997) 197–201.
[4] T. Berther, G.H. Gautschi, J. Kubler, Capacitive accelerometers for static and low-frequency measurements, Sound and Vibration 30 (6) (1996) 28–30.
[5] D.W. Stachell, J.C. Greenwood, A thermally-excited silicon accelerometer, Sens. Actuators 17 (1989) 241–245.
[6] R.L. Kubena, G.M. Atkinson, W.P. Robinson, F.P. Stratton, A new miniaturized surface micromachined tunneling accelerometer, IEEE Electron Device Lett. 17 (6) (1996) 306–308.
[7] U.A. Dauderstadt, P.H.S. de Vries, R. Hiratsuka, P.M. Sarro, Silicon accelerometer based on thermalpiles, Sens. Actuators A 46/47 (1995) 201–204.
[8] E. Abbaspour-Sani, R.S. Huang, C.Y. Kwok, A wide-range linear optical accelerometer, Sens. Actuators A 49 (1995) 149–154.
[9] H. Takao, Y. Matsumoto, M. Ishida, Stress-sensitive differential amplifiers using piezoresistive effects of MOSFETs and their application to three-axial accelerometers, Sens. Actuators A 65 (1998) 61–68.
[10] P.L. Chen, R.S. Muller, R.D. Jolly, G.L. Halac, R.M. White, A.P. Andrews, T.C. Lim, M.E. Motamedi, Integrated silicon microbeam PI-FET accelerometer, IEEE Trans. Electron Devices ED-29 (1) (1982) 27–33.
[11] P. Scheeper, J.O. Gullov, L.M. Kofoed, A piezoelectric triaxial accelerometer, J. Micromech. Microeng. 6 (1996) 131–133.
[12] D.L. Polla, L. F Francis, Ferroelectric thin films in microelectromechanical systems applications, MRS Bull. 21 (7) (1996) 59–65.
[13] M. Okuyama, Microsensors and microactuators using ferroelectric thin films, Proceedings of the International Symposium on Micromechatronics and Human Science, Nagoyz, Japan, Nov 25–28 1998, 29–34.
[14] B. Kloeck, S.D. Collins, N.F. de Rooij, R.L. Smith, Study of electrochemical etch-stop for high-precision thickness control of silicon membranes, IEEE Trans. Electron Devices 36 (4) (1989) 663–669.
[15] J. Fricke, E. Obermeier, Cantilever beam accelerometer based on surface micromachining technology, J. Micromech. Microeng. 3 (1993) 190–192.
[16] S.K. Ha, C. Keilers, F.K. Chang, Finite element analysis of composite structures containing distributed piezoceramic sensors and actuators, AIAA J. 30 (3) (1992) 772–780.
[17] A.F. Vaz, Composite modeling of flexible structures with bonded piezoelectric film actuators and sensors, IEEE Trans. Instrum. Measurement 47 (2) (1998) 513–520.
[18] R.P. van Kampen, R.F. Wolffenbuttel, Modeling the mechanical behavior of bulk-micromachined silicon accelerometers, Sens. Actuators 64 (1998) 137–150.
[19] Y. Nemirovsky, A. Nemirovsky, P. Muralt, N. Setter, Design of a novel thin-film piezoelectric accelerometer, Sens. Actuators 56 (1996) 239–249.
[20] E.O. Doebelin, Measurement Systems Application and Design, 4th Edition, McGraw-Hill, New York, 1990, pp. 258–264.
[21] H. Seidel, L. Csepregi, A. Heuberger, H. Baumgartel, Anisotropic etching of crystalline silicon in alkaline solution, J. Electrochem. Soc. 137 (11) (1990) 3612–3626.
[22] W. Lang, Silicon microstructuring technology, Mater. Sci. Eng. R17 (1996) 1–55.
[23] T.B. Gabrielson, Mechanical–thermal noise in micromachined acoustic and vibration sensors, IEEE Trans. Electron Devices 40 (5) (1993) 903–909.
[24] J. Yu, C. Lan, System modeling and robust design of microaccelerometer using piezoelectric thin film, in: Proceedings of the 1999 IEEE International Conference on Multisensor Fusion and Integration for Intelligent Systems, Taipei, ROC, August 1999, pp. 99–104.

Biographies

Jyh-Cheng Yu received the BS degree in 1985 from the Department of Mechanical Engineering, National Taiwan University, ROC, and the MS degree in 1990 and PhD degree in 1994 from the Department of Mechanical Engineering, the Ohio State University, USA. In 1995, he worked in the field of precision parts design at the Industrial Technology Research Institute, ROC. He has been an Associate Professor in the

Department of Mechanical Engineering at the National Taiwan University of Science and Technology since 1996. His research interests include Design and Manufacturing of Microsensors, Engineering Optimization, Quality Engineering, and Concurrent Engineering.

Chin-Bing Lan received the BS degree in 1997 and the MS degree in 1999 from the Department of Mechanical Engineering, National Taiwan University of Science and Technology, ROC. His MS thesis studied the system modeling and robust design of microsensors using ferroelectric thin film. Currently, he is a Mechanical Engineer at the Electron Materials Department of the Nan-Ya Plastics Corporation working in the field of liquid crystal display.